Integrated Solar Power Harvesting and Hibernation for a Recurrent-Mission VTOL Micro Aerial Vehicle

Stephen J. Carlson*, Tolga Karakurt, Prateek Arora, Christos Papachristos

Abstract—This work addresses the electronics and behaviors of a Hibernation-Enabled Maximum-Power-Point-Tracking power converter and power management system. This enables a Recurrent-Mission profile that can be performed by VTOL Micro Aerial Vehicles for persistent presence in real-world unstructured environments. The typical mission cycle consists of solar energy harvesting while the vehicle is landed and in an energy-conserving state, followed by a vertical take-off and entry into forward flight when the battery is fully charged. The flight mission is concluded with a vertical landing and entry into hibernation for the process to repeat indefinitely, for multiple instances each day and through the night to the next day. The presented MPPT implementation demonstrates a functional prototype and the successful demonstration of a multi-day mission cycle using our open-access Tricopter/Fixed-Wing Vertical Take-Off and Landing MAV.

I. INTRODUCTION

Over the past several years, aerial robots have evolved to fill niches in various markets and environments. These devices can be found being used in personal, industrial[1–6], military and search-and-rescue roles [7–10]. Aerial robots are also used in exploration tasks in both earth-bound [11–17] and extra-planetary ventures, such as the Mars Ingenuity Helicopter [18] and various planned missions [19, 20].

Following the example demonstrated by the Mars Ingenuity Helicopter, there exists a nascent niche in earth-based flying robots, for both terrestrial and oceanic cases, wherein in-situ solar energy harvesting capability can be leveraged to extend presence and mission duration indefinitely. The critical distinction is that the mission cycle consists of long periods of solar-charging hibernation, punctuated by flights that use the stored energy to accomplish mission goals such as surveying an area or repositioning of the vehicle. At the conclusion of each flight, the vehicle lands and hibernates while harvesting solar energy to repeat the cycle. We term this process in small UAVs as migratory behavior [21], as it imitates the same paradigm that migratory bird species use the world over for traversing their respective environments. This can also be rendered as "recurrent-mission" behavior; we will use both terms interchangeably in this paper. Such a system becomes capable of unsupervised long-term autonomous operation, in the sense of recurrently executing flight missions without having a human or any specialized infrastructure tend to its energy needs.

This material is based upon work supported by the NSF Award: AWD-01-00002751: RI: Small: Learning Resilient Autonomous Flight. The presented content and ideas are solely those of the authors.

The authors are with the University of Nevada, Reno, 1664 N. Virginia, 89557, Reno, NV, USA stephen_carlson@nevada.unr.edu



Fig. 1. The MiniHawk-VTOL, a Tri-TiltRotor hybrid aircraft equipped with onboard solar energy harvesting for migratory (recurrent-mission) behavior demonstration.

The utility of the recurrent mission profile is evident when considering that many operation environments preclude ground support infrastructure or human assistance to the flying robot. An aerial robot crossing over oceans or through access-denied regions cannot utilize pre-placed charging stations or landing sites, as is common with "Drone-in-a-Box". While a solar-powered High-Altitude, Long-Endurance (or "HALE") aircraft can solve this problem, such a vehicle must remain airborne indefinitely, both day and night, continuously powering the propulsion system as any off-field landing away from an established ground-support site is typically fatal to the aircraft. This forces the HALE concept to fly above the weather, and typically with narrow margins for payload and operation domain. With the migratory mission profile, a less complex and more cost-effective vehicle can traverse the same environment as the HALE concept, but with less sensitivity to the reduction of solar energy due to season or weather, and with no obligation to continuously expend energy for propulsion.

The critical enabling mechanisms to demonstrate the migratory mission cycle are as follows: First, a small UAV must be capable of self-mobility and locomotion for launching into flight and landing without reliance upon any ground-based infrastructure; only a VTOL-capable design can satisfy this requirement. Second, such a vehicle must have a solar array that can accumulate solar energy; the input rate is of minor concern, so long as there is a definite positive accumulation of energy for the typical illumination of the mission daytime

^{*} Consider for Best Student Paper Award

environment. Third and finally, the energy that is captured should be able to be stored efficiently with minimal perishability. This is accomplished with two devices: A Maximum-Power-Point-Tracking DC-DC Converter, and a Hibernation-Capable Battery Management and Power Switching System.

Considering the above critical elements for enabling the migratory mission cycle, some hurdles are presented. While VTOL platforms are somewhat common, as are solar-powered fixed-wing vehicles, what is rare if at all existent is a small UAV design that incorporates solar cells into the wings of a fixed-wing VTOL vehicle. Responding to this deficiency, we have previously designed and released, for open-access, our own Solar-enabled VTOL platform, the MiniHawk-VTOL. While this platform solves the first (VTOL) and second (Solar-Powered) elements necessary for the migratory mission cycle, a Hibernation-Capable combined MPPT, Battery Management, Power Switching System is novel at this moment in the aerial robotics field. The design and implementation of such a device is the subject of this work.

This paper is partitioned as follows: Section II addresses background and research related to migratory behaviors in small UAVs. Section III demonstrates the theory and implementation details for designing a hibernation-capable energy harvesting system. Experimental results are shown in Section IV, and our conclusions are drawn in Section V.

II. RELATED WORK

There exist various examples of unattended robots using solar energy harvesting. As previously identified, the Mars Ingenuity Helicopter [18] uses a solar array and hibernating power system, and this provides the only fully realized reference of a hibernating flying robot. Other projects have postulated or attempted the same, notably, experiments by The University of Minnesota [22, 23], a tiltrotor by MIT [24], The University of Michigan Flying-Fish [25], and the Sherbrooke University SUWAVE [26, 27]. All of these offer modern examples of solar migratory behavior, but each fall short of describing the hibernation-enabling device design.

Relaxing scope to include examples of non-hibernating solar-powered flying robots yields the Airbus Zephyr and the ETH AtlantikSolar Project [28], the later being particularly useful in informing the design of our own device. As a general reference for the design of switching power converter electronics, we used [29], which provides details on designing most types of DC-DC switching regulators.

III. SYSTEM DESIGN

This section will describe the design and implementation of the Hibernation-Capable MPPT for recurrent mission behaviors. The three main innovations of the Hibernation-Capable MPPT system are as follows:

 A Solid-State Relay is incorporated into the device, for switching the aircraft battery in and out of the entire aircraft power system.

- 2) A Low-power design that allows for the least amount of energy consumption during periods of hibernation with no solar energy input.
- An interface to the aircraft autopilot or other host computer system for setting wake-up timers or wake conditions, and measures to ensure that hibernation is not commanded erroneously.

These elements are described below, along with various other supporting elements and design considerations.

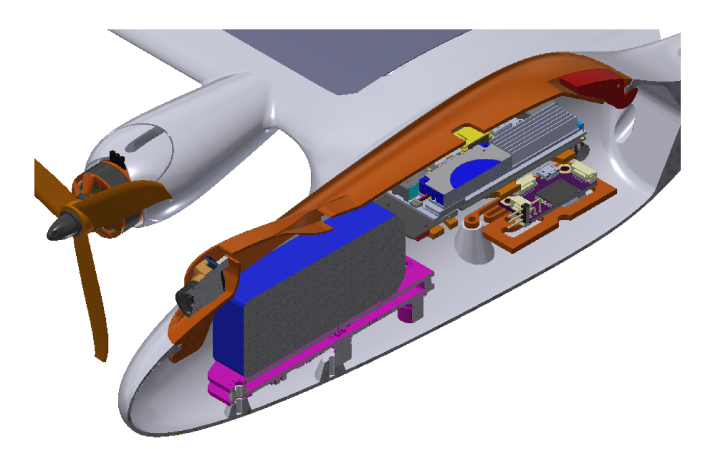


Fig. 2. MiniHawk-VTOL Assembly with the MPPT electronics (magenta) beneath the Lipoly Battery (blue).

A. Target Aircraft Design and Characteristics

Many of the constraints driving the design of this Hibernation-Capable MPPT are determined by the characteristics of the host aircraft. In this case, we are targeting the MiniHawk-VTOL, which is our in-house rapidlyprototyped VTOL UAV of the operationally versatile [30, 31] Tri-Tiltrotor class [32-36]. The aircraft is designed specifically for demonstrating the basic migratory behavior set with minimal complexity and cost, and as such, it is not optimized for carrying a larger solar array, or for efficient fixed-wing flight. Thus, while it does implement a wingembedded solar array using the highly efficient MaxeonTM C60 flexible cell form-factor, it only employs a necessary minimum of four $153cm^2$ cells (providing 14W in the best case). This may change in a future revision of the design, allowing for a greater number of solar cells. The aircraft in its current iteration has a wingspan of 800mm, and weighs about 1kg. The aircraft design has been documented in [37,

An important factor that necessitates the hibernation behavior is that the avionics used by the MiniHawk-VTOL are common commercial off-the-shelf devices, all of which are not designed for entering a low-power state. For example, the Electronic Speed Controllers that pull from the aircraft power bus do not support commands for entering a shutdown state, and so each device will contribute some parasitic intrinsic load while present on the supply bus. The same goes for the autopilot, which, while open-source, still presents a complex

electronic system with many design elements that cannot be shutdown to conserve power. Thus, it is necessary to switch the entire aircraft power bus from upstream near the battery.

The MPPT device is designed to fit within the existing vehicle. Figure 2 shows the MiniHawk-VTOL sectioned along the avionics bay, with the MPPT placed under the battery. The volume reservations for the device are length=100mm, width=50mm and thickness=10mm.

Proceeding from the reference points above, and with the aircraft components known, and with future optimizations to the host aircraft in mind, the MPPT must observe the following constraints:

- 1) The MPPT must be able to charge up to a 4s (16.8V) Lipoly Battery, with preference for up to 6s (25.2V).
- 2) The MPPT must be able to draw from a MaxeonTM C60 array, consisting of a string of 4 series-connected cells, with preference for extending this to an array of 24 series-connected cells. This yields a range starting at 2.4V for the 4-cell case, up to 15V for the 24-cell case. The electrical current developed on the string may exceed 6A.
- 3) Given the high angular dynamics of the aircraft, the solar array can experience fast changes in the incident solar radiation vector. Therefore, the tracking loop should adjust the converter duty cycle fast enough to prevent severely over-shooting or under-shooting the Maximum Power Point, but also, if a software-defined ideal diode is implemented, quick changes to incident radiation must not be allowed to back-drive the solar array.
- 4) The mass of the Hibernation-Capable MPPT must be as low as possible, preferably less than 50 grams.
- 5) To fit within the avionics bay, the dimensions of the MPPT must not exceed 50mm width, height must not exceed 10mm, and length should not exceed 100mm.
- 6) The MPPT must be able to disconnect the entire aircraft power bus from the battery, given the high quiescent current that the autopilot and propulsion avionics draw when powered.
- 7) The MPPT itself must draw the least amount of quiescent power possible when hibernation has been entered and solar energy is deficient for charging.

The following section will detail the actual MPPT hardware design, as informed by the above constraints. The behavior of the MPPT software and communication are shown in Section III-C.

B. Electronics Design

As shown in Figure 3, the MPPT interfaces with the solar array, battery, the aircraft power bus, and the autopilot via a serial connection. Each power connection is measured for current and voltage. The MPPT microcontroller and its associated power regulator are not shown in the diagram and are implicit.

1) MPPT Topology: The DC-DC converter topology used in the MPPT is a combined Buck-Boost converter, using four switching MOSFETS in a H-bridge configuration, with

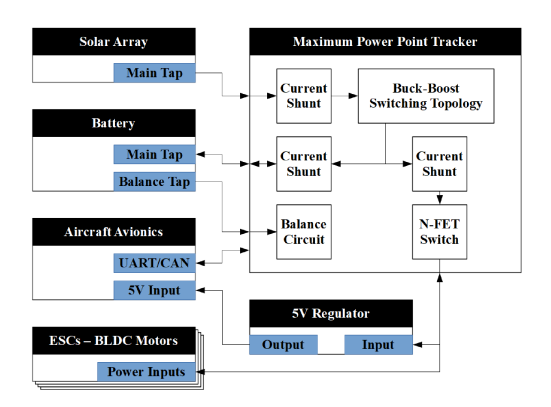


Fig. 3. MPPT Block Diagram.

"High-side" and "Low-side" devices on each side of an inductor. The reason for selecting this configuration is due to the aircraft-contributed constraints above, where the input voltage may be higher than the output voltage, and vice versa. With this configuration, for either the Buck (Step-Down) Mode, or the Boost (Step-Up) Mode, one side of the bridge is non-switched and remains static, while the other side is switched.

The Buck-Boost topology allows for Synchronous switching, wherein, for each conduction cycle, the forward-conducting (or "Synchronous") MOSFET can be turned on to emulate an ideal diode during the complementary phase. This greatly increases the efficiency of the converter when compared to a traditional diode-based design. This mode can be degraded to a Non-synchronous switching mode to prevent back-driving the solar input, such as in the case where the converter nears operation in a discontinuous state.

The Buck-Boost switching MOSFETs are chosen to be N-channel devices, as these have the highest performance compared to P-channel devices. The voltage rating of the MOSFETs is fixed by the expected input and output voltage with adequate safety margin, which for the requirements drawn above, yields a value of 40V.

The use of N-channel Power MOSFETs requires that each High-Side device is driven by a bootstrap driver to exceed the $V_{GS(th)}$ voltage needed to turn the device on. To accommodate this need, and to prevent shoot-through of the H-bridge switches, each side of the H-bridge is driven by a Synchronous Half-Bridge Gate Driver IC. The Gate Driver IC output characteristics are interactive with some of the parameters of the MOSFETS, such as maximum Gate Charge Q_g and Gate Threshold Voltage $V_{GS(th)}$, so Gate Driver selection requires observing MOSFET compatibility. This interaction also determines the switching frequency and corresponding switching losses of the converter.

The maximum efficient switching frequency above also interacts with the inductor selection: Ideally, we would prefer as large an inductor as possible so that switching frequency can be as low as possible to minimise the switching losses, but only to a point; the device must not exceed the requirements for volume and mass. Selecting a smaller inductor requires that the switching frequency is increased.

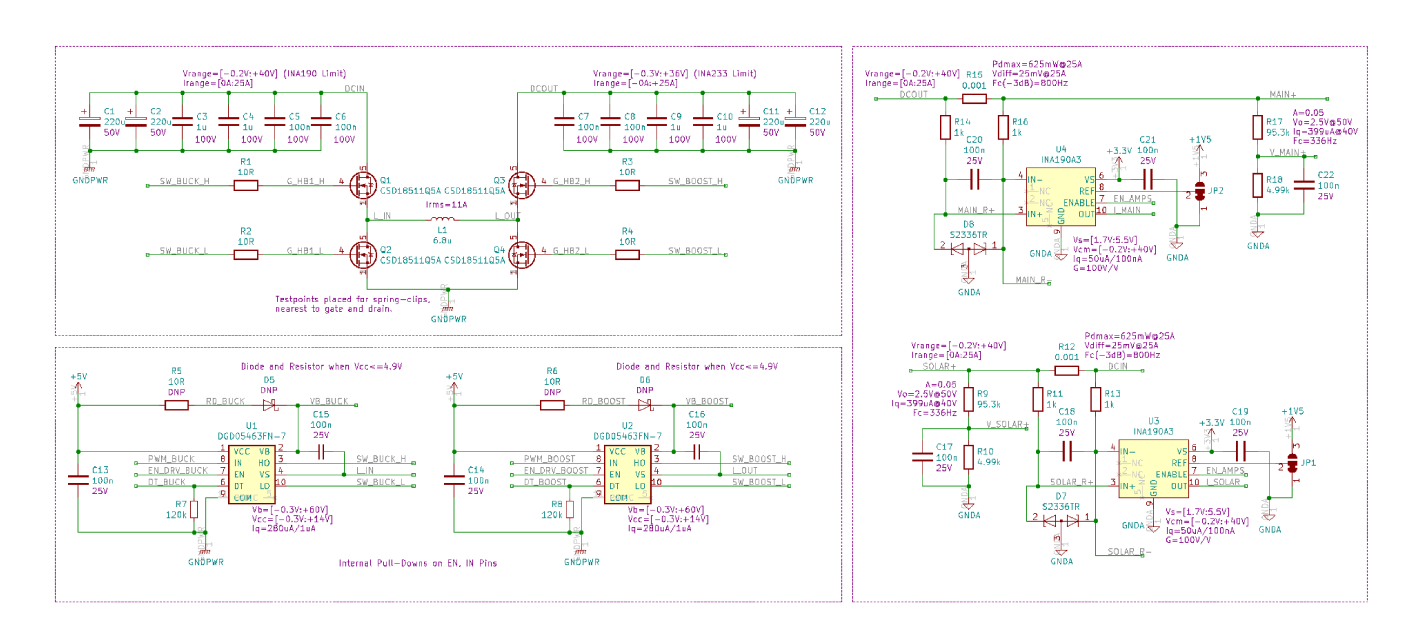


Fig. 4. MPPT System Schematic. Upper-Left: DC-DC Switched Power Path Topology. Lower-Left: MOSFET Drivers. Right: Analog Sensing Domain.

A table of some of the final component selections are reflected in Table I. The Power Path is shown in the upper-left partition of Figure 4, and the MOSFET Drivers are shown in the lower-left partition.

TABLE I
MPPT BILL OF MATERIALS

Part	Value	Qty
Power MOSFETs	TI CSD18511Q5A	4
MOSFET Drivers	DI DGD05463FN-7	2
Current Sense Amplifiers	TI INA190A3	2
TVS Diodes	SMC S2336TR	2
Inductor	Bourns SRP1245A-6R8M	1
Microcontroller	SparkFun ESP32 Thing	1
Opto-Isolator	IXYS CPC5001	1
Solid-State Relay	Emcotec EMCA72006-F	1

- 2) Analog Sensing: The analog voltage sensing on the MPPT is provided by resistive voltage dividers. These are anti-aliasing filtered and buffered prior to being read by the microcontroller ADC inputs. Analog current sensing is accomplished with rail-to-rail current-sense amplifiers, sensing the differential voltage across precision current-shunt resistors. These devices can measure positive and negative current flow. The right partition of Figure 4 shows the Analog Sensing domain. Note that while resistive dividers and shunts dissipate power when compared to Hall effect sensing, the overhead is minimal for sufficiently large resistive divider values and sufficiently small shunt values.
- 3) Microcontroller and Power Regulator: The MPPT prototype uses the Espressif ESP32TM, a popular IoT device with several useful peripherals. The device can host microSD and MMC Flash devices for logging data, and has a full IP and RF stack for wireless connectivity. However, the essential peripherals used are the PWM outputs, ADC inputs, and UART serial ports. The MOSFET Drivers are driven from the PWM outputs, and all analog sensing channels are ingested by the ESP32. This device is powered with a 5V switching

regulator with low quiescent load. The ESP32 is able to deep-sleep and reduce input power below 10uA. An important note: The serial connection between the aircraft avionics and ESP32 is opto-isolated to protect the MPPT microcontroller from backdriving the aircraft avionics during hibernation. Figure 5 shows the CAD model and finished system when attached to the microcontroller and 5V regulator.



Fig. 5. *Left*: 3D Model of the DC-DC Powerpath and Sensory Board. *Right*: The feature-complete MPPT coupled with an ESP32 microcontroller.

- 4) Solid-State Relay: For the MPPT prototype, we use a commercially-available Solid-State Relay designed for R/C aircraft. An interface was adapted between this device and the MPPT microcontroller such that the relay is only switched off when two GPIOs from the ESP32 are asserted HIGH and LOW respectively. Pull-up and pull-down behavior prevents this selection in cases where one or both of the GPIOs from the host microcontroller float. When the relay is switched off, the quiescent current drops below measurable levels.
- 5) Battery Balancer: For the MPPT prototype, we use a commercially-available Lithium Polymer battery balancer circuit board, which is attached directly to the battery balance leads. This device does not contribute meaningful quiescent current when idle, and can sustain over 1A of balancing load to cells that become unbalanced.

C. System Behavior

The ESP32 runs a version of FreeRTOS, providing a real-time operating environment. This allows for running two real-time tasks concurrently; the *MPPT* Task, and the *Command* Task. Each task can forward information to the other using Message Queues. The following sections describe activities of each task, and the interactions between tasks.

1) MPPT Task Behavior: The MPPT Task is responsible for taking measurements from the ESP32 ADC peripheral, performing statistics on the measurements, and using the filtered measurements for its own Maximum-Power-Point-Tracking algorithm, and forwarding these measurements periodically to the Command task. After power-up and initialization, the MPPT Task starts in the Idle state. The Idle state inactivates the DC-DC converter by driving PWM outputs to Low, and commanding the MOSFET Drivers to sleep.

A message from the Command Task can trigger the transition from the Idle State to the Ramp Initialize state, usually when the Command Task determined that the Lipoly battery was present on the system, and that the solar input power was sufficient to merit charging. The Ramp Initialize State and subsequent Ramp State sample the entire I-V curve of the solar array, from short-circuit to open-circuit. A histogram data structure is populated with this curve, and the global power maximum is found with the corresponding duty-cycle setpoint that produced it. This setpoint value is fed to the MPPT Initialize State as a seed value for the perturb-and-observe algorithm. As the perturb-and-observe algorithm only finds the local maxima, sampling the entire I-V space every 100 seconds helps to avoid operation outside of the global maximum power point. The MPPT duty-cycle setpoint is quickly reduced if the battery voltage reaches the ceiling (16.8V) or if safe output current is exceeded. The converter remains active until the Command Tasks triggers the Idle State by setting the Power State variable to false. Figure 6 shows the state machine diagram.

2) Command Task Behavior: The Command Task transacts serial communication and configures system state. As described above, this task receives the measurement data from the MPPT Task and replies via the Message Queue with commands to start or stop charging, based on the presence of the battery and solar state. This task also initiates waking from hibernation when the system timer reaches a previously set alarm value, or if the battery voltage exceeds a given threshold.

The Command Task has the ability to initiate Hibernation, but the process is thoroughly safeguarded, as an accidental entry into hibernation could be disastrous during flight. Thus, a two-step verification process is used. First, a request is generated by the autopilot or host computer using a Hibernation Request message. This message payload contains the requested number of minutes to sleep; if zero, then the MPPT will only wake the aircraft when the battery is fully charged. The MPPT response to the hibernation request message repeats the requested sleep timer, and additionally provides an arbitrary pesudo-random value as a "challenge"

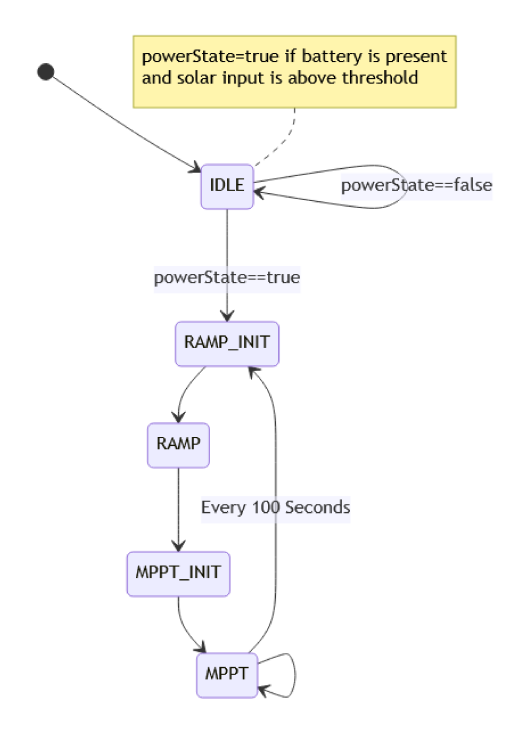


Fig. 6. MPPT DC-DC Converter State Machine.

or verification code. The autopilot or host computer has a window of 200ms to respond, this time replying using a Hibernation Response message, which again consists of the desired sleep time and the verification code that was sent by the MPPT. If the MPPT receives the response message, and all fields match between the initial and final request, hibernation will be initiated. This scheme guards against the request being corrupted by transmission errors, as each device has the opportunity to review and confirm the action. Figure 7 shows the sequence diagram.

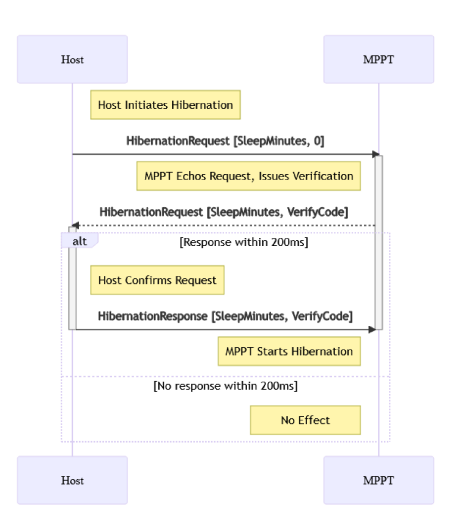
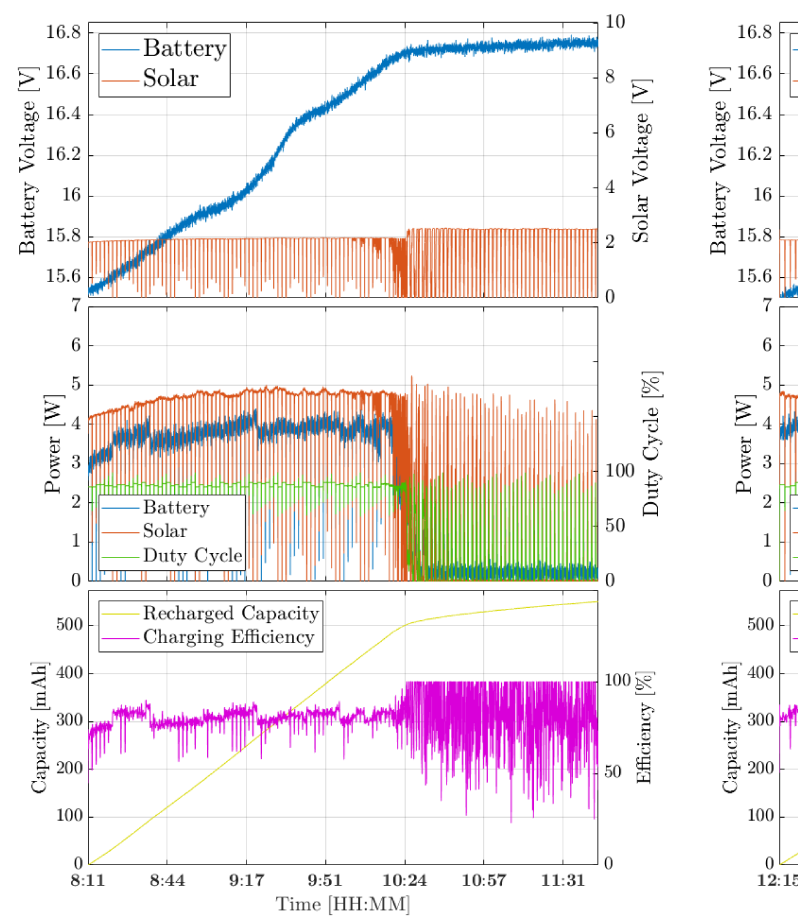


Fig. 7. Hibernation Initiation Sequence.



First cycle - Indicative solar-powered self-recharging at early morning hours (8 am to 12 noon)

Efficiency 13:55 12:15 12:48 14:28 Time [HH:MM] Fig. 9. Second cycle - Indicative solar-powered self-recharging at afternoon hours (12 noon to 3 pm) commands the MPPT to hibernate, either for an arbitrary duration or until the vehicle battery is fully charged. In hibernation, the vehicle autopilot and propulsion avionics are

Solar Voltage [V]

Duty Cycle [%]

100 🔄

0

Battery

Solar

Battery

Duty Cycle

Recharged Capacity

Charging Efficiency

Solar

IV. EXPERIMENTAL STUDY

To demonstrate the proposed recurrent mission behaviors, we devised a multi-cycle mission profile. For each day of testing, the aircraft was flown for each occurrence of the battery reaching full-charge. The experiment preparations involved installing the MPPT prototype inside of the avionics bay of a solar-winged MiniHawk-VTOL vehicle, inserting the device between the battery and the power input connection of the vehicle propulsion and avionics systems. The wing-mounted solar cells were connected to the MPPT, and the isolated serial connection to the vehicle autopilot was attached.

For conducting each test, the mission process is sequenced by a script running on the vehicle autopilot, with each step gated by a permissive safety switch on the vehicle's R/C controller. (This permissive gating is only necessary in initial testing, and is expected to be removed as experiments continue.) Upon vehicle power-up and initialization, the sequence script arms the vehicle and enters the autonomous flight mode, which begins a pre-programmed waypoint mission. This mission is followed until either the mission has been fully completed, or a low battery failsafe is encountered. In either case, the vehicle starts a Return-to-Land sequence. Upon successfully landing and disarming, the sequence script

fully disconnected from the battery.

We successfully performed recurrent mission behavior in various environmental conditions; in instances of both overcast and clear conditions. For these experiments, the waypoint mission was configured to only have the vehicle hover in-place indefinitely, as a practical measure to ease logistics in attending the vehicle while at rest, and to keep the vehicle within safe boundaries. For this indefinite positionhold hover, the vehicle reverts to the Return-to-Land behavior upon Low Battery, as described above. The effect is the same in terms of energy consumed, regardless of the type of mission performed.

The experiment shown in Figure 8 and Figure 9 demonstrates a day with three flights performed; the first flight occurred at 08:00, immediately preceding the beginning of Figure 8. At 12:00, a second flight occurred, immediately after the end of the first plot and preceding the start of data of Figure 9. A third and final flight for the day was accomplished after the end of Figure 9. The plots show artifacts from the MPPT 100-second-recurrent I-V curve estimation sweep, appearing as transient dips; other artifacts include a

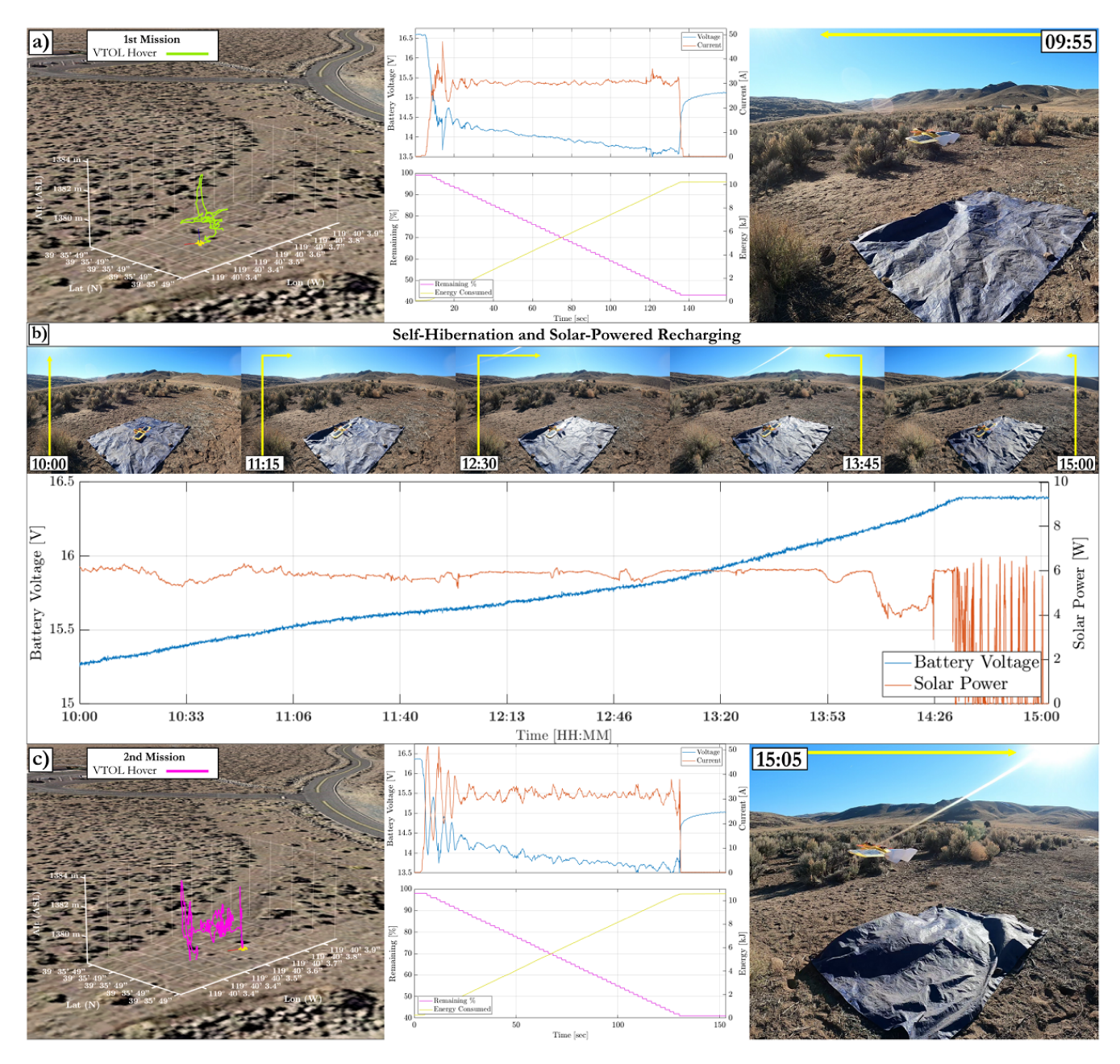


Fig. 10. Recurrent Mission Demonstration. *1st Mission* consists of *a*) VTOL climb and position hold, followed by *b*) VTOL landing. The aircraft battery is disconnected from the avionics via the ESP32-controlled SSR (hibernation), and energy is accumulated until *c*) *2nd* (*Recharged*) *Mission* starts with *e*) VTOL climb, hover, and VTOL landing. A corresponding experimental video is provided as supplementary material with this paper.

tree branch shading the aircraft for the period near 13:20, and the full-battery behavior can be seen following charge completion at 10:30 and approximately 14:45, respectively.

The experiment shown in Figure 10 demonstrates another example of the recurrent mission. As with Figure 8 and Figure 9, this series represents the solar charge behavior, but also includes the battery behavior of the hovering flights preceding and following the energy harvesting session. For the entire ensemble of experiments presented, the concept of multi-day recurrent mission behavior is shown as viable.

V. CONCLUSIONS

This paper proposed and demonstrated the utility, design and build process of a Hibernation-Capable MPPT power

system, for achieving a recurrent multi-day mission profile. The relationships between the host aircraft and the new design were shown, with constraints for size, weight, and quiescent sleep power illustrated. The high-level principles for the parts and design patterns were discussed. It was shown that the system autonomously decides when to enter hibernation and power harvesting modes, as well as autonomous wake up when its battery supply is recharged to resume its mission. The Schematic, Bill of Materials and other artwork are shown, with the intent to contribute the design to as an open-access and open-source project.

REFERENCES

- [1] M. Burri, J. Nikolic, C. Hürzeler, G. Caprari, and R. Siegwart, "Aerial service robots for visual inspection of thermal power plant boiler systems," in 2012 2nd international conference on applied robotics for the power industry (CARPI). IEEE, 2012, pp. 70–75.
- [2] A. Bircher, K. Alexis, M. Burri, P. Oettershagen, S. Omari, T. Mantel and R. Siegwart, "Structural inspection path planning via iterative viewpoint resampling with application to aerial robotics," in *IEEE International Conference on Robotics and Automation (ICRA)*, May 2015, pp. 6423–6430.
- [3] C. Papachristos, K. Alexis, L. R. G. Carrillo, and A. Tzes, "Distributed infrastructure inspection path planning for aerial robotics subject to time constraints," in 2016 international conference on unmanned aircraft systems (ICUAS). IEEE, 2016, pp. 406–412.
- [4] F. Mascarich, T. Wilson, C. Papachristos, and K. Alexis, "Radiation source localization in gps-denied environments using aerial robots," in 2018 IEEE International Conference on Robotics and Automation (ICRA). IEEE, 2018, pp. 6537–6544.
- [5] S. Khattak, C. Papachristos, and K. Alexis, "Visual-thermal landmarks and inertial fusion for navigation in degraded visual environments," in 2019 IEEE Aerospace Conference. IEEE, 2019, pp. 1–9.
- [6] C. Papachristos and K. Alexis, "Augmented reality-enhanced structural inspection using aerial robots," in 2016 IEEE international symposium on intelligent control (ISIC). IEEE, 2016, pp. 1–6.
- [7] N. Michael, S. Shen, K. Mohta, Y. Mulgaonkar, V. Kumar, K. Nagatani, Y. Okada, S. Kiribayashi, K. Otake, K. Yoshida et al., "Collaborative mapping of an earthquake-damaged building via ground and aerial robots," *Journal of Field Robotics*, vol. 29, no. 5, pp. 832–841, 2012.
- [8] M. Tranzatto, F. Mascarich, L. Bernreiter, C. Godinho, M. Camurri, S. M. K. Khattak, T. Dang, V. Reijgwart, J. Loeje, D. Wisth, S. Zimmermann, H. Nguyen, M. Fehr, L. Solanka, R. Buchanan, M. Bjelonic, N. Khedekar, M. Valceschini, F. Jenelten, M. Dharmadhikari, T. Homberger, P. De Petris, L. Wellhausen, M. Kulkarni, T. Miki, S. Hirsch, M. Montenegro, C. Papachristos, F. Tresoldi, J. Carius, G. Valsecchi, J. Lee, K. Meyer, X. Wu, J. Nieto, A. Smith, M. Hutter, R. Siegwart, M. Mueller, M. Fallon, and K. Alexis, "Cerberus: Autonomous legged and aerial robotic exploration in the tunnel and urban circuits of the darpa subterranean challenge," *Journal of Field Robotics*, 2021.
- [9] T. Tomic, K. Schmid, P. Lutz, A. Domel, M. Kassecker, E. Mair, I. L. Grixa, F. Ruess, M. Suppa, and D. Burschka, "Toward a fully autonomous uav: Research platform for indoor and outdoor urban search and rescue," *IEEE robotics & automation magazine*, vol. 19, no. 3, pp. 46–56, 2012.
- [10] P. Arora and C. Papachristos, "Mobile manipulation-based deployment of micro aerial robot scouts through constricted aperture-like ingress points," in 2021 IEEE/RSJ International Conference on Intelligent Robots and Systems (IROS), 2021, pp. 6716–6723.
- [11] S. Khattak, C. Papachristos, and K. Alexis, "Keyframe-based direct thermal-inertial odometry," in 2019 International Conference on Robotics and Automation (ICRA). IEEE, 2019, pp. 3563–3569.
- [12] S. Khattak, C. Papachristos, and K. Alexis, "Keyframe-based thermal-inertial odometry," *Journal of Field Robotics*, vol. 37, no. 4, pp. 552–579, 2020.
- [13] S. Khattak, F. Mascarich, T. Dang, C. Papachristos, and K. Alexis, "Robust thermal-inertial localization for aerial robots: A case for direct methods," in 2019 International Conference on Unmanned Aircraft Systems (ICUAS). IEEE, 2019, pp. 1061–1068.
- [14] T. Dang, F. Mascarich, S. Khattak, H. Nguyen, N. Khedekar, C. Papachristos, and K. Alexis, "Field-hardened robotic autonomy for subterranean exploration," Field and Service Robotics (FSR), 2019.
- [15] C. Papachristos, S. Khattak, and K. Alexis, "Uncertainty-aware receding horizon exploration and mapping using aerial robots," in 2017 IEEE international conference on robotics and automation (ICRA). IEEE, 2017, pp. 4568–4575.
- [16] C. Papachristos, M. Kamel, M. Popović, S. Khattak, A. Bircher, H. Oleynikova, T. Dang, F. Mascarich, K. Alexis, and R. Siegwart, "Autonomous exploration and inspection path planning for aerial robots using the robot operating system," in *Robot Operating System* (ROS). Springer, Cham, 2019, pp. 67–111.
- [17] C. Papachristos, F. Mascarich, S. Khattak, T. Dang, and K. Alexis, "Localization uncertainty-aware autonomous exploration and mapping with aerial robots using receding horizon path-planning," *Autonomous Robots*, vol. 43, no. 8, pp. 2131–2161, 2019.

- [18] J. Balaram, M. Aung, and M. P. Golombek, "The ingenuity helicopter on the perseverance rover," *Space Science Reviews*, vol. 217, no. 4, pp. 1–11, 2021.
- [19] W. Johnson, S. Withrow-Maser, L. Young, C. Malpica, W. Koning, K. WJF, M. Fehler, A. Tuano, A. Chan, A. Datta et al., Mars Science Helicopter Conceptual Design. National Aeronautics and Space Administration, Ames Research Center, 2020.
- [20] R. D. Lorenz, E. P. Turtle, J. W. Barnes, M. G. Trainer, D. S. Adams, K. E. Hibbard, C. Z. Sheldon, K. Zacny, P. N. Peplowski, D. J. Lawrence et al., "Dragonfly: A rotorcraft lander concept for scientific exploration at titan," *Johns Hopkins APL Technical Digest*, vol. 34, no. 3, p. 14, 2018.
- [21] S. J. Carlson and C. Papachristos, "Solar energy harvesting for a land-to-recharge tiltrotor micro aerial vehicle," in 2022 IEEE Aerospace Conference (AEROCONF), 2022.
- [22] R. D'Sa, D. Jenson, T. Henderson, J. Kilian, B. Schulz, M. Calvert, T. Heller, and N. Papanikolopoulos, "Suav: Q-an improved design for a transformable solar-powered uav," in 2016 IEEE/RSJ International Conference on Intelligent Robots and Systems (IROS). IEEE, 2016, pp. 1609–1615.
- [23] R. D'Sa, T. Henderson, D. Jenson, M. Calvert, T. Heller, B. Schulz, J. Kilian, and N. Papanikolopoulos, "Design and experiments for a transformable solar-uav," in 2017 IEEE International Conference on Robotics and Automation (ICRA). IEEE, 2017, pp. 3917–3923.
- [24] J. T. VanderMey, "A tilt rotor uav for long endurance operations in remote environments," Ph.D. dissertation, Massachusetts Institute of Technology, 2011.
- [25] R. Eubank, E. Atkins, and G. Meadows, "Unattended operation of an autonomous seaplane for persistent surface and airborne ocean monitoring," in OCEANS 2010 MTS/IEEE SEATTLE. IEEE, 2010, pp. 1–8.
- [26] R.-A. Peloquin, D. Thibault, and A. L. Desbiens, "Design of a passive vertical takeoff and landing aquatic uav," *IEEE Robotics and Automation Letters*, vol. 2, no. 2, pp. 381–388, 2016.
- [27] É. Tétreault, D. Rancourt, and A. L. Desbiens, "Active vertical takeoff of an aquatic uav," *IEEE Robotics and Automation Letters*, vol. 5, no. 3, pp. 4844–4851, 2020.
- [28] A. Noth, "Design of solar powered airplanes for continous flight," Ph.D. dissertation, ETH Zurich, 2008.
- [29] S. S. Ang, Power-switching converters. M. Dekker, 1995.
- [30] C. Papachristos, K. Alexis, and A. Tzes, "Technical activities execution with a tiltrotor uas employing explicit model predictive control," *IFAC Proceedings Volumes*, vol. 47, no. 3, pp. 11036–11042, 2014.
- [31] S. J. Carlson, P. Arora, and C. Papachristos, "A multi-vtol modular aspect ratio reconfigurable aerial robot," in 2022 IEEE International Conference on Robotics and Automation (ICRA), 2022.
- [32] C. Papachristos, K. Alexis, and A. Tzes, "Design and experimental attitude control of an unmanned tilt-rotor aerial vehicle," in 2011 15th International Conference on Advanced Robotics (ICAR). IEEE, 2011, pp. 465–470.
- [33] C. Papachristos and A. Tzes, "Modeling and control simulation of an unmanned tilt tri-rotor aerial vehicle," in 2012 IEEE International Conference on Industrial Technology. IEEE, 2012, pp. 840–845.
- [34] C. Papachristos, K. Alexis, and A. Tzes, "Towards a high-end unmanned tri-tiltrotor: Design, modeling and hover control," in 2012 20th Mediterranean Conference on Control & Automation (MED). IEEE, 2012, pp. 1579–1584.
- [35] C. Papachristos, K. Alexis, and A. Tzes, "Model predictive hovering-translation control of an unmanned tri-tiltrotor," in 2013 IEEE International Conference on Robotics and Automation. IEEE, 2013, pp. 5425–5432.
- [36] C. Papachristos, K. Alexis, and A. Tzes, "Dual-authority thrust-vectoring of a tri-tiltrotor employing model predictive control," *Journal of intelligent & robotic systems*, vol. 81, no. 3-4, pp. 471–504, 2016
- [37] S. J. Carlson and C. Papachristos, "The MiniHawk-VTOL: Design, modeling, and experiments of a rapidly-prototyped tiltrotor uav," in 2021 International Conference on Unmanned Aircraft Systems (ICUAS). IEEE, 2021, pp. 777–786.
- [38] S. J. Carlson and C. Papachristos, "Migratory behaviors, design principles, and experiments of a vtol uav for long-term autonomy," ICRA 2021 Aerial Robotics Workshop on "Resilient and Long-Term Autonomy for Aerial Robotic Systems", 2021. [Online]. Available: https://www.aerial-robotics-workshop.com/uploads/5/8/4/4/ 58449511/icra2021-aerial_paper_8.pdf